Indian Journal of Pure & Applied Physics
Vol. 45, June 2007, pp. 549-554

Structural and magnetic properties of zinc ferrite aluminates synthesized by ceramic method

Suman* & N D Sharma**

*Department of Physics, Kurukshetra University, Kurukshetra 136119
**Department of Electronics and Communication Engineering,
J M Institute of Enginering and Technology, Radaur 135 133

Received 27 June 2006; revised 29 December 2006; accepted 10 January 2007

Mössbauer spectroscopy has been used to investigate the cation distribution in $ZnAl_xFe_{2-x}O_4$ spinel ferrites with the composition $0 \le x \le 1$. All samples were prepared using the ceramic technique. A single phase formation of the compounds did not occur. It is confirmed by X-ray diffraction measurements. The variation in saturation magnetization of the samples at room temperature has been explained on the basis of site distributions and the strength of the exchange interactions between magnetic ions.

Keywords: Structural properties, Magnetization, Mössbauer spectroscopy, Zinc ferrite aluminates, Ceramic technique
IPC Code: G01J 3/12

1 Introduction

Zinc ferrite aluminates $ZnAl_xFe_{2-x}O_4$ with composition ($0 \le x \le 1$) were synthesized at 1300°C using the usual ceramic method. Since structural and magnetic properties of ferrites are highly sensitive to the impurity levels present in them, extensive work has been reported on different aspects to improve the performance of basic ferrites[1-3]. When the composition of ferrites is modified by adding varying amounts of impurities, it is obvious that the distribution of the magnetic ions and the resultant magnetic moments are affected. The change in synthesis temperature of ferrites results in redistribution of iron cations, which updates the crystal properties, such as macroscopic magnetisation[4-6]. In this paper, the effect of Al^{3+} substitution has been studied in $ZnAl_xFe_{2-x}O_4$ with $0 \le x \le 1$ at room temperature. The cation redistribution in copper ferromagnets by X-ray, Mössbauer spectroscopy and magnetization technique has been determined.

2 Experimental Details

Samples of $ZnAl_xFe_{2-x}O_4$ ferrites with $0 \le x \le 1$ were prepared by double sintering ceramic process. Stoichiometric mixtures of pure powders, iron oxide (Fe_2O_3), aluminium oxide (Al_2O_3) and zinc oxide (ZnO) were calcined at 1000°C for 12 h. These were then compacted by dry pressing in steel dies to obtain pellet form. The pellets were sintered at 1150°C for 12 h. The samples so obtainrd were ball-milled for 3 h at the rate of 90 rpm and again pellets were formed. These pellets were sintered at 1300°C and then slowly cooled down to room temperature at a rate of 2°C /min.The samples have been investigated by XRD using CuK_α radiation on a Philips PW (1710) diffractrometer. The Mossbauer spectroscopy analysis has been carried out at room temperature in a standard transmission geometry, using ^{57}Co source in Rh matrix. Isomer shifts were measured relative to α-Fe. The magnetization measurements (M versus H) of all samples were carried out at room temperature using vibrating sample magnetometer (VSM). However, M versus T for all the samples was carried out in the temperature range 87- 300K.

3 Results and Discussion

Six samples of the mixed spinel system $ZnAl_xFe_{2-x}O_4$; x = 0.0, 0.2, 0.4, 0.6, 0.8 and 1.0 were studied. In each sample Zn remained at its regular lattice site while Fe was replaced by aluminium.

3.1 X-ray measurements

Fig.1 shows powder diffraction patterns for all samples. The appearance of the planes (012), (220), (104), (311), (113), (400), (024), (422), (116) (333), (440), (214), (620) and (533) shows the cubic spinel ferrite phase with hematite (γ-Fe_2O_3). The reflection

corresponding to hematite phase is due to preferential loss of Zn^{2+} ions under firing process, The divalent Zn is more volatile and has low melting point[7-8]. It may be added that we prepared the samples twice and got similar results. At lower values of x, ferrites and hematite peaks are not distinguishable exactly but at higher values the peaks can be easily detected. Lattice parameters were calculated from the position of the principal peaks using a standard least squares routine computer program and are shown in Table 1. The lattice constant a (Å) of the series $ZnAl_xFe_{2-x}O_4$ plotted as a function of x is shown in Fig. 2. It is observed that this series obeys the Vegard's law. The variation of lattice constant a (Å) with Al content x can be explained on the basis of difference in ionic radii of the constituent ions. The decrease in lattice constsnt a with increasing x is due to the fact that the smaller Al^{3+} (0.51Å) ions replace larger Fe^{3+} (0.64Å) ions in the spinel structure.

The X-ray density (d_X) for each sample was calculated by the relation:

$$d_X = Z\,M / N\,V$$

where Z is the number of molecules per unit cell (Z= 8), M molecular weight, V unit cell volume and N is Avogadro's number. The compositional dependence of the X-ray density (d_x) is shown in Fig. 3. The X-ray density (d_X) decreases with increasing aluminium concentration x. This is because the decrease in mass overtakes the decrease in volume of the unit cell.

3.2 Magnetisation measurements

The magnetization measurements (M versus H) of all samples were carried out at 300 K using vibrating sample magnetometer (VSM). A variation of magnetization with applied field at 300K is presented in Figs 4-6. The typical characteristic of a ferromagnetic behaviour i.e. a hystersis loop is observed for the sample x=0.0,0.2,0.4. However, for the other samples, saturation magnetization was calculated by extrapolating the magnetization versus the inverse of the field i.e $1/H$ curve to $1/H = 0$. On addition of non-magnetic Al^{3+} ions in place of iron ions, the hystersis loop i.e. the ferromagnetic

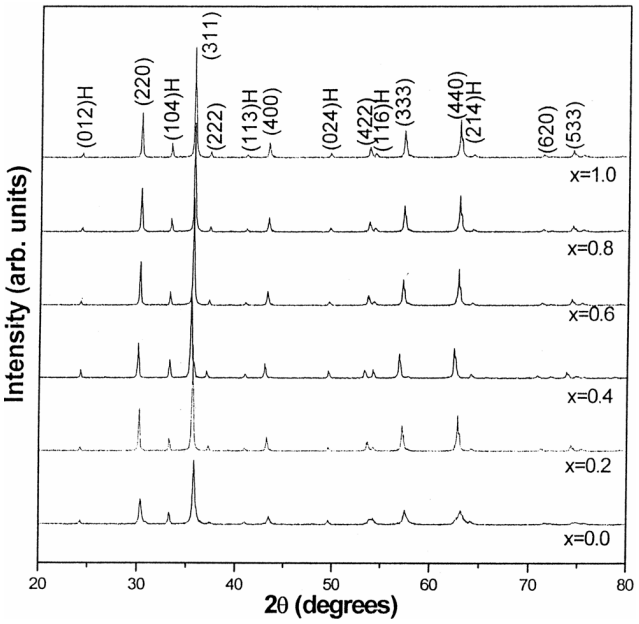

Fig. 1—Typical XRD pattern for $ZnAl_xFe_{2-x}O_4$ system

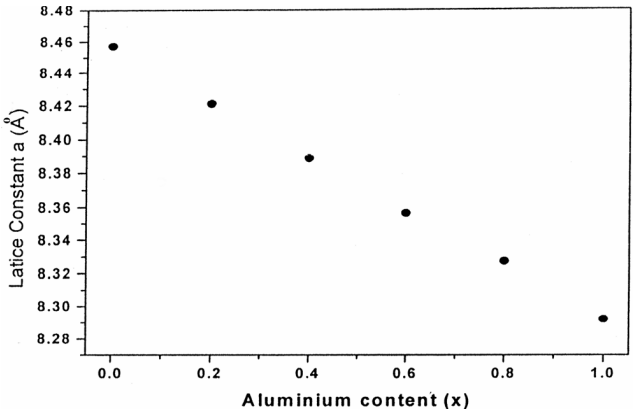

Fig. 2—Variation of lattice constant a (Å) with aluminum content (x)

Table1—Lattice constant, X-ray density, saturation magnetization, magneton number for $Zn\,Al_x\,Fe_{2-x}\,O_4$ ferrite system.

Content x	Lattice constant a (Å)	X-Ray Density (d_x)	σ_s (emu/gm) 300 K	n_B (μ_B) 300 K
0.0	8.45721	5.2919	1.78	0.069
0.2	8.42137	5.2308	1.59	0.048
0.4	8.38893	5.1612	1.45	0.041
0.6	8.35664	5.0893	—	—
0.8	8.32739	5.0097	1.01	0.032
1 .0	8.29214	4.9387	0.89	0.021

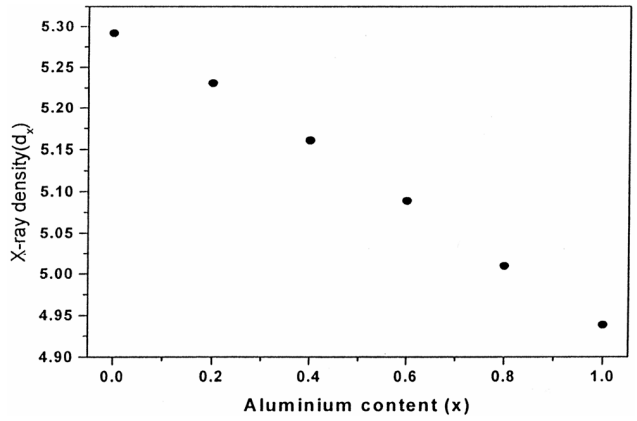

Fig. 3—Variation of X- ray Density with aluminium content (x)

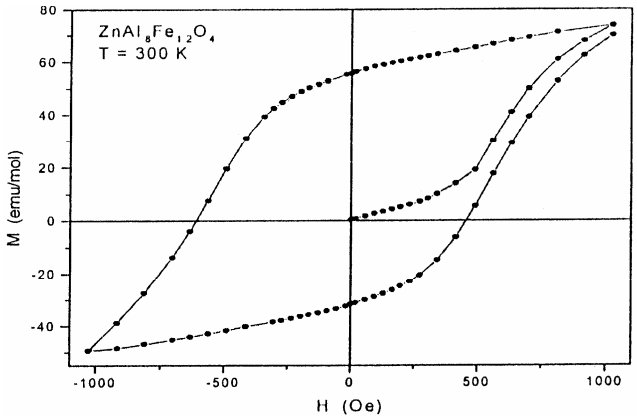

Fig. 5—Field dependence of magnetization curve for $ZnAl_{0.8}Fe_{1.2}O_4$

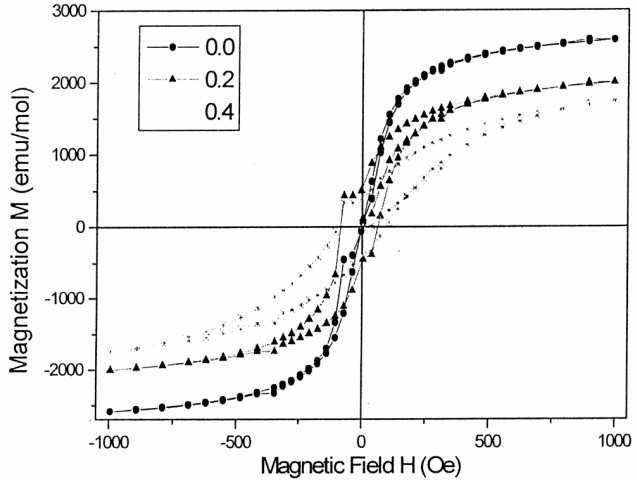

Fig. 4—Field dependence of magnetization curve for $ZnAl_xFe_{2-x}O_4$ for x=0.0,0.2,0.4

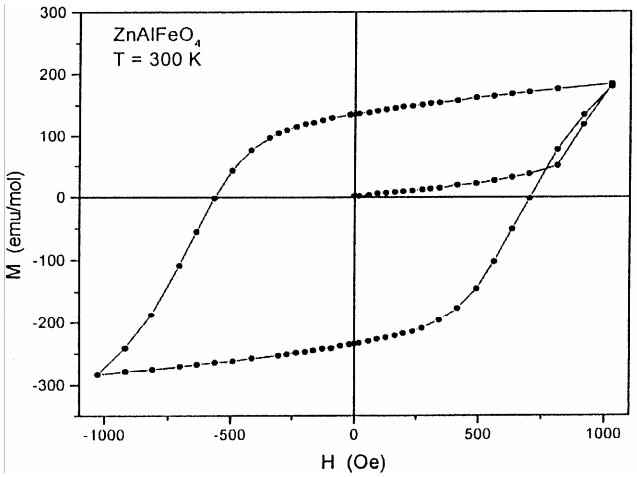

Fig. 6—Field dependence of magnetization curve for $ZnAlFeO_4$

character starts dominating further. This is due to the fact that α-Fe_2O_3 is not completely oxidized into ferrite phase because zinc oxide which helps in the formation of ferrite, is lost (some of its amount) during firing process as Zn has lower melting point and low vapour pressure. However, the remaining amount of zinc oxide is not compatible for the complete ferrite formation. The X-ray results also show the existence of extra peaks of α-Fe_2O_3 in addition to the ferrite phase. The second reason is also that the crystal structure of γ-Fe_2O_3 is as that of corundum α-Al_2O_3 and shows a ferromagnetic character at room temperature. Moreover, the saturation magnetization decreases with increasing Al^{3+} ion concentration. To explain the composition dependence of magnetization, the concept of cation distribution may be taken into account. Since zinc ferrite is a normal spinel, the possible cation distribution can be represented as follows :

$$(Zn^{2+}\ Fe^{3+})\ [Fe^{3+}]O_4^{-2}$$

where the first and the second brackets indicate tetrahedral (A-site) and octahedral (B-site) sublattice respectively. The replacement of Fe^{3+} ions by Al^{3+} ions having magnetic moment $0\mu_B$ wherein 85 % of $Al^{3+}(x)$ ions occupy B-sites while remaining 15% go to A-sites[9-10], this gives $(1-x+y)Fe^{3+}$ ions on A-site and $(1-x)Fe^{3+}$ ions on the B-site. Then, the possible distribution of cations will take the form:

$$(Zn^{2+}\ Al_x^{3+}\ Fe_{1-x}^{3+})[Al^{3+}Fe_{1-x}^{3+}]O_4^{-2} \qquad \ldots (1)$$

The ionic magnetic moment of Zn^{2+} 'y' (non-magnetic) is $0\mu_B$ and the magnetic moment of Fe^{3+} is $5\mu_B$. Therefore, the substitution of Al^{3+} leads to decrease in the Fe^{3+} ions concentration at B-site and consequently the magnetization due to B-sites will

decrease. At the same time the magnetization of A-site will also decrease with the decreasing Fe^{3+} ion concentration on A-sites. Accordingly, the net magnetization will decrease. The magneton number (n_B) was calculated from the hystersis loop (*M-H* curve) obtained at 300K by the following relation[11] :

n_B = molecular weight × saturation magnetization / 5585

The variation of n_B [the saturation magnetization per formula unit in Bohr magneton (μ_B)] was obtained from hysteresis loop technique as a function of Al concentration and is presented in Table 1. From the field dependence of magnetization and the observed magnetic moments at room temperature, it is evident that n_B decreases with increase of aluminium concentration. According to Neel's two sublattice model[12], the magnetic moment per formula unit, η_B^N, with the known cation distribution at A and B sites is given by following equation :

$$\eta_B^N = M_B(x) - M_A(x) \quad \ldots (2)$$

where η_B^N is the Neel magnetic moment per formula unit in μ_B , M_B and M_A are, respectively, the B and A sublattice magnetic moments in μ_B. The $\eta_{B(x)}^N$ is the calculated value of magnetic moment using Neel's model and x is dopant concentration. The possible values of magnetic moment per formula unit ($\eta_{B(x)}^N$) calculated from Neel's model on the basis of cation distribution for x = 0.0 to 1.0 and using Eq. (2) are given in Table 1. The calculated ($\eta_{B(x)}^N$) values for x = 0.0 to 1.0 disagree with the experimentally found n_B values (Table 1). This result indicates that significant canting of spins exists on B sites leading to a non-collinear [9,13-15] type of magnetic structure.

3.3 Mössbauer measurements

Mössbauer absorption spectra for all the samples i.e. x = 0.0, 0.2, 0.4, 0.6, 0.8 and 1.0 were recorded at room temperature and are shown in Fig. 7 (a to f). The spectra were computer fitted and the hyperfine parameters are listed in Table 2. The Mössbauer spectra exhibit a broad asymmetric sextet along with a central doublet. The central doublet in all the samples arises due to the presence of non-magnetic zinc ions[12-14] as well as incomplete oxidation of hematite into ferrite phase[15]. All the spectra were fitted with three sextets and a single quadrupole doublet. Because of overlap in the sextets, one has to use the

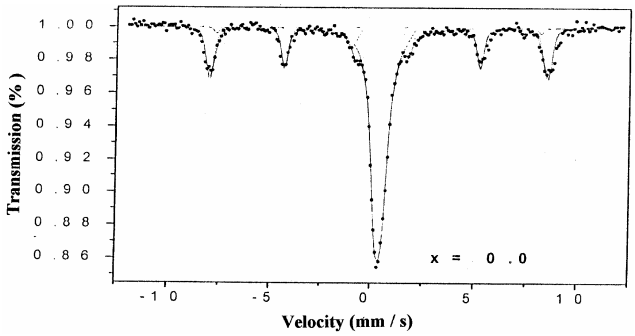

Fig. 7(a)—Mössbauer absorption spectrum at 300K for x = 0.0

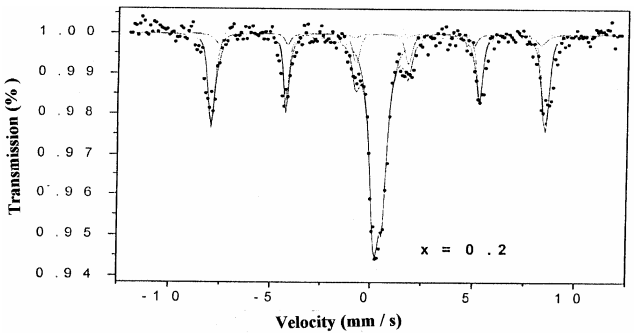

Fig. 7(b)—Mössbauer absorption spectrum at 300K for x = 0.2

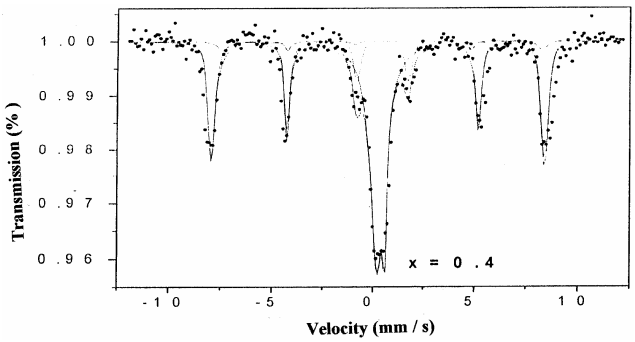

Fig. 7(c)—Mössbauer absorption spectrum at 300K for x = 0.4

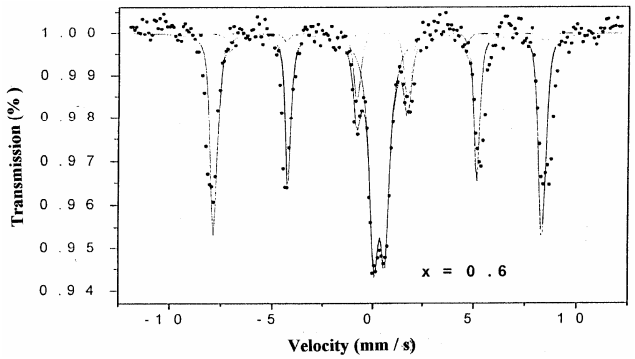

Fig. 7(d)—Mössbauer absorption spectrum at 300K for x = 0.6

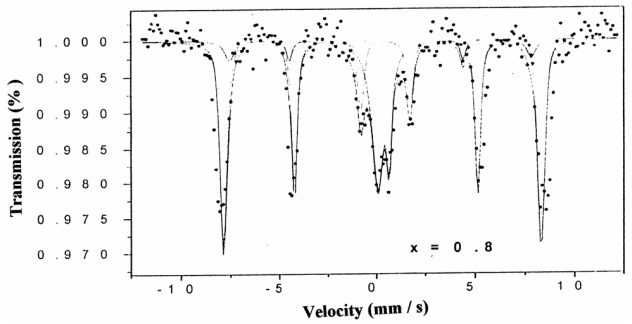

Fig. 7(e)—Mössbauer absorption spectrum at 300K for $x = 0.8$

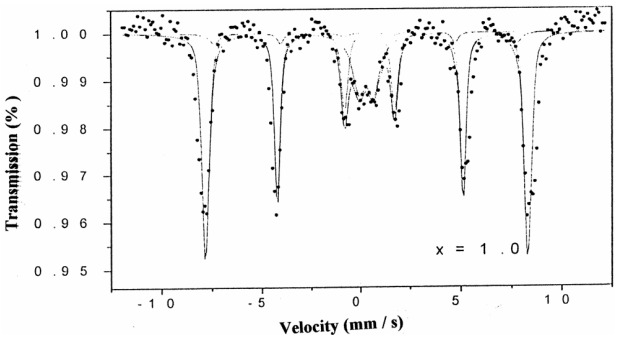

Fig. 7(f)—Mössbauer absorption spectrum at 300K for $x = 1.0$

Table 2—Hyperfine interaction parameters computed from the Mössbauer absorption spectra recorded at room temperature, isomer shift is given relative to α–Fe

Content x	Site	I S ($\delta \pm 0.01$) mm/s	Q S ($\Delta \pm 0.01$) mm/s	Area ± 0.2 mm/s	H_{int} ± 2.0 T
	H	0.34	-0.12	13.09	52.5
0.0	B	0.36	-0.21	16.21	51.1
	A	0.30	-0.16	10.33	50.0
	D	0.32	0.39	60.37	—
	H	0.33	-0.13	16.50	52.1
0.2	B	0.38	0.28	24.73	50.9
	A	0.32	0.11	10.62	49.8
	D	0.30	0.42	48.15	—
	H	0.35	-0.18	19.01	52.0
0.4	B	0.38	-0.32	28.50	50.7
	A	0.30	-0.02	12.28	49.5
	D	0.28	0.48	40.21	—
	H	0.34	-0.16	22.16	51.8
0.6	B	0.36	-0.36	32.54	50.4
	A	0.27	-0.05	18.22	49.2
	D	0.26	0.62	27.08	—
	H	0.36	-0.21	23.16	51.7
0.8	B	0.38	-0.33	37.54	50.3
	A	0.30	-0.06	21.22	48.6
	D	0.26	0.68	18.08	—
	H	0.34	-0.21	25.01	51.5
1.0	B	0.38	-0.29	40.83	50.1
	A	0.26	-0.04	23.23	48.4
	D	0.24	0.71	10.93	—

constraint of line widths. The outemost sextet is attributed to a crystalline component i.e. γ-Fe_2O_3 phase, whereas inner sextets, are due to the Fe^{3+} ions at the octahedral (B) site and the other due to the Fe^{3+}ions at the tetrahedral (A) site. It is well known[14] that Zn^{2+} has marked preference only for tetrahedral (A) sites, whereas iron and alminium ions co-exist at both A and B-sites, however, they prefer B-sites. On increasing the alminium concentration, the outermost sextet becomes more intense as compared to the other two sextets. This shows that ferrite formation is not in a single phase, which is also supported by X-ray studies. As the alminium concentration is increased, the paramagnetic doublet decreases indicating a reduction of the $ZnFeO_2$ (delafossite) phase[16,17]. Similar results have also been observed in copper ferrite aluminates[17-18]. The value of isomer shift due to Fe^{3+} ions at tetrahedral (A) and octahedral (B) sites (Table 1) shows no significant change which indicates that the s-electron density at the Fe^{3+} nucleus is not affected by Al^{3+} substitution. The hyperfine field decreases with increasing Al^{3+} ion concentration (x) in $ZnAl_xFe_{2-x}O_4$ system. The decrease in the value of H_{hf} with x can be explained on Neel's molecular field theory and super transferred hyperfine field mechanism. The super transferred hyperfine field at

Fe^{3+} ion at the B-site is due to spin transfer from the d-orbitals of the nearest-neighbour cations which-occupy the B-site through the ligand anions to the s-orbitals of the Fe^{3+}(A) ion. Thus, the super transferred hyperfine field at the A-site will depend on the magnetic moment of the B-site. Due to the site preference, the Al^{3+} ions prefer the B-sites and the substitution of Fe with the non-magnetic Al^{3+} ions, results in replacing Fe ions from A and B-sites simultaneously.

This reduces the magnetization at both sites and in turn reduces the super transferred hyperfine field. Such a variation can be explained qualitatively, zinc ferrite ($ZnFe_2O_4$) has normal spinel structure and the diamagnetic ions (Zn^{2+}) occuping A-sites, allow only weak B-B interaction[19]. On addition of Al^{3+} ions in place of iron ions, as Al^{3+} ions have got a strong tendency to occupy B-sites, it reduces AB interaction with increase in Al^{3+} concentration. As the Al concentration is increased, the BB super transferred hyperfine interactions become comparable in strength because of canting of spins (non-collinear). These BB super transferred hyperfine interactions are strongly dependent on the spins and therefore reduce the net hyperfine field[20-23]. It is also evident from the Mössbauer absorption spectra that there is systematic decrease in the internal hyperfine field H_{in} values with the increasing alminium substitution[24,25]. This happens because the replacement of larger Fe^{3+} ions (0.64Å) by smaller Al^{3+} ions (0.51Å) affects the internal hyperfine fields at the nearest Fe^{3+} sites through transferred hyperfine fields. The results observed reveal that the intensity and the area of all the three sextets increase, however, the area of the paramagnetic doublet corresponding to $ZnFeO_2$ (delafossite) phase decreases on increasing non-magnetic Al^{3+} ion concentration. Such observations suggest that the ferromagnetic character increases on increasing Al^{3+} ion concentration.

4 Conclusion

The system $ZnAl_xFe_{2-x}O_4$ (x = 0.0,0.2,0.4) shows a weak ferromagnetic behaviour. The magnetic behaviour starts dominating further i.e. the system shows clear hystersis loop when the value of x approaches 1.0. The values of magnetic moment per formula unit in Bohr magneton obtained from *M-H* curve decrease with increasing Al^{3+} ion concentration. These results are also in good agreement with Mössbauer measurements. Mössbauer studies also show that there exists a $ZnFeO_2$ delafossite phase besides the main matrix $ZnAl_xFe_{2-x}O_4$. It is thus concluded that a non-collinear magnetic structure exists and the complete formation of the ferrite phase does not occur in the present system.

Acknowledgement

The authors are grateful to Dr N P Lalla, and Dr. Alok Banerji, Scientist, UGC-DAE, facilities for scientific research (Indore Centre) for their help in carrying out XRD and magnetization measurements, respectively.

References

1 Oliver S A, Harris V G, Hamdeh H H & Ho J C, Appl Phys Lett , 76 19 (2000) 2761.
2 Yafet Y, Kittal C, Phys Rev B, 87 (1952) 290.
3 Drmann J I & Nogus M, J Phys Conden Matt, 2 (1990) 1223.
4 Parvatheeswara Rao B, Subha Rao P S V & Rao K H, IEEE Trans Magn, 33 6 (1997) 4454.
5 Das A R, Ananthan V S & Khan D C, J Appl Phys, 57 (1985) 4189.
6 Ata-Allah S S & Fayek M K, J Phys Chem Solids, 61 (2000) 1529.
7 Amer M A, Phys Status Solidi (a) ,181 (2000) 539.
8 Chander Rath, Anand S, Das R P, Kulkarni S D, Date S K & Mishra N C, J Appl Phys, 91 4 (2002) 2211.
9 Whinfrey C G, Eckort D W & Tauber A, J Am Chem Soc, 82 (1960) 2695.
10 Lee Sung Ho & Kim Woong Tae, J Phys: Condens Matter, 4 (1992) 8245.
11 Kale A, Gubbala S & Misra R D K, J Magn & Magn Mater, 277 (2004) 350.
12 Thummer K P, Chhantbar M C, Modi K B, Baldha G J & Joshi H H, J Magn & Magn Mater, 280 (2004) 23.
13 Modi Kunal B, Joshi H H & Kulkarni R G, Indian J Pure & Appl Phys, 34 (1996) 92.
14 Yang De Ping, Lavoie Lindsey K, Zhang Yide, Zhang Zongalo & Shinhui Ge, J Appl Phys, 93 (10) (2003).
15 Das Dipankar, Indian J Phys, 78 A 2 (2004) 185.
16 Kulkarni R G, Trivedi Bimal S, Joshi H H & Baldha G J, J Magn & Magn Mater, 159 (1996) 375 .
17 Almokhtar M, Abdalla Atef M & Gaffar M A, J Magn & Magn Mater, 272-276 (2004) 2216.
18 Greenwood N N & Gibb T C, Mössbauer Spectroscopy, (Chapman and Hall Ltd London), 1971.
19 Srivastava M C, Shringi S N & Srivastava R G, Phys Rev B, 14 (1976) 2041.
20 Rao A D P, Raju S B, Vadera S R & Sharma D R, Bull Matel Sci, 26 5 (2003) 505.
21 Suman, Roshan Lal, Sharam N D, Taneja S P & Gupta Ajay, Indian J Pure & Appl Phys, 43 (2005) 44.
22 Suman & Sharam N D ,Indian J Pure & Appl Phys, 44 (2006) 220.
23 Almokhtar M, Abdalla Atef M & Gaffar M A, J Magn Magn Mater, 272-276 (2004) 2216.
24 Kulkarni R G, Bimal S Trivedi, Joshi H H & Baldha G J, J Magn Magn Mater 159 (1996) 375.
25 Srivastava M C, Shringi S N & Srivastava R G, Phys Rev B, 14 (1976) 2041.